THE DESIGN OF EDDY-CURRENT MAGNET BRAKES

Der-Ming Ma, Jaw-Kuen Shiau
Department of Aerospace Engineering, Tamkang University, Danshuei, Taiwan 25137, Republic of China
E-mail: derming@mail.tku.edu.tw

Received December 2009, Accepted December 2010
No. 09-CSME-73, E.I.C. Accession 3159

ABSTRACT

The eddy-current is created by the relative motion between a magnet and a metal (or alloy) conductor. The current induces the reverse magnetic field and results in the deceleration of motion. The proposed mechanism implements this phenomenon in developing a braking system. The potential applications of the braking system can be a decelerating system to increase the safety of an elevator or any guided rail transportation system. To provide scientific investigation for industrial application of magnetic braking, this study presents four systematic engineering design scenarios to design a braking system. The constant magnetic field is the simplest and easiest design to implement. The optimal magnetic field distribution is obtained by minimizing the deceleration effort. The piecewise-constant magnetic field distribution offers a compromise between performance and magnetic field requirements. The advantages of the section-wise guide rail are tolerable deceleration; and simple design requirement and manufacturing processes. In the study, an experimental braking system using constant magnetic field is build to demonstrate the design procedure.

Keywords: Magnetic brakes; eddy-current magnetic brakes; optimum control.

LA CONCEPTION DE SYSTÈMES DE FREINAGE MAGNÉTIQUES À COURANTS DE FOUCAULT

RÉSUMÉ

Les courants de Foucault sont crées par le mouvement relatif entre un champ magnétique et un métal (ou un alliage) conducteur. Le courant provoque l'induction du champ magnétique inverse et produit la décélération du mouvement. Le mécanisme proposé met en œuvre ce phénomène pour le développement d'un système de freinage. Les applications potentielles pourraient être la base d'un système de décélération en vue de l'accroissement de la sécurité d'un élévateur-transporteur ou de tout système guidé sur rail. Dans le but de contribuer à la recherche scientifique pour l'application industrielle d'un système de freinage magnétique, cet article présente quatre scénarios pour la conception d'un système de freinage. Le champ magnétique permanent est le plus simple et facile à concevoir. La distribution optimale du champ magnétique est obtenue en réduisant l'effort de décélération. La distribution permanente par section d'un champ magnétique offre un compromis entre la performance et les conditions requises du champ magnétique. Les avantages offerts sont la décélération tolérable, la simplicité de la conception et des procédés manufacturiers. Pour les fins de la recherche, un système de freinage expérimental utilisant un champ magnétique permanent a été construit pour démontrer la procédure employée.

Mots-clés : freinage magnétique; freinage magnétique à courants de Foucault; contrôle optimal.

1. INTRODUCTION

Most of the braking systems utilize friction forces to transform the kinetic energy of a moving body into heat that is dissipated by the braking pads. The overuse of friction-type braking systems causes the temperature of the braking pads to rise, reducing the effectiveness of the system. The relative motion between the magnet and the metal (or alloy) conductor produces an eddy current that induces a reverse magnetic field and results in deceleration. Without using friction, an eddy-current braking system transforms the kinetic energy of the moving body into heat energy that is dissipated through the eddy current in the conductor. However relative velocities between the magnet and the conductor are required to activate an eddy-current braking system. Because of the simplicity of this mechanism, it can be used as a decelerator or auxiliary braking system to ensure the safety of system.

Studies on the actuation of electro-mechanical machines using an eddy current can be traced back to the early 20th century. The mathematical description of the eddy current induced in a conductor under varying magnetic fields is rather complicated. Therefore, in developing eddy current braking systems, designers usually make certain assumptions to allow a simple mathematical representation of the magnetic field. This makes it possible to derive the analytic solution of the induced eddy current distribution caused by the interaction between the moving conductor and the magnetic field. The eddy current braking force can then be computed accordingly. References [1–4] all fall under this category. Researchers currently use finite element analysis tools to approximately compute magnetic fields and eddy current distribution [5].

In this study, four systematic engineering design scenarios to design a braking system are presented: a constant magnetic field, an optimal magnetic field distribution, piecewise-constant magnetic fields and a section-wise guide rail with a constant magnetic field. The constant magnetic field is the simplest and easiest design to implement. Furthermore, the constant magnetic field can be generated by utilizing permanent magnet to achieve a nearly maintenance-free system. Figure 1 shows the experimental magnetic braking system using constant magnetic field. This experimental constant magnetic field braking system consists of two parts: guided rails and a mass-lifter assembly (Fig. 2). The rails, made of the 6061 alloy, guide the mass up and down. Pure copper is chosen as the conductor. Magnets passing through the conductor induce an eddy current in the copper, inducing drag that decreases motion. To achieve better performance, the smaller gaps between the copper and magnets are required. To reduce the deformation of the copper strips, they are divided into sections (Fig. 3). The magnets are installed on the back of the mass in three U-type containers (Fig. 4). Each U-type container is rigid enough to withstand strong magnetic forces and remain un-deformed. Figure 5 is the cross-section view of the braking medium. Referring to Fig. 5, the thickness of the copper is 5.27 mm; and the gap between the copper and the magnet is 6 mm.

In this experiment, a hydro-powered lifter was used to lift the mass. Upon reaching the top of guided rail, a hook on the upper back of the mass grabbed a hook at the top of the structure, holding the mass to the top. A small hydro-powered pusher then released the hook on the top to drop the mass as a free-falling object. Since the magnitude of the magnetic braking force depends on the relative velocity of the rail and the mass-lifter assembly, an absorber was needed to absorb the impact of the mass.

Based on the magnetic braking system above, we used the approximate mathematic model of the magnetic field to derive the braking force caused by the eddy current.

Fig. 1. The experimental braking system.

2. THE DESIGN OF CONSTANT MAGNETIC FIELD BRAKING SYSTEM

Consider the setup depicted in Fig. 6. In this figure, a permanent magnet is moving along a stationary conducting plate, inducing an electric field with intensity, $\vec{E} = \vec{B} \times \vec{u}$, on the conducting plate and producing circulating eddy currents. $\vec{E}$ is in the direction of the vector $\vec{B} \times \vec{u}$, $\vec{B}$ is the magnetic field on the conducting plate created by the permanent magnet, and $\vec{u}$ is the velocity of the moving permanent magnet. We assume that the air gap between the permanent magnet and the conducting plate is very thin (compared to the size of the magnet).

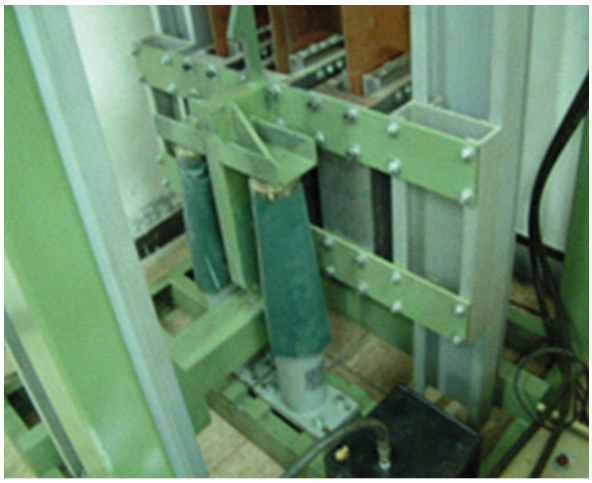

Fig. 2. The lifter.

Therefore, the magnetic field is uniform inside the magnet pole projection area on the conducting plate and zero outside the magnet pole projection area. According to Ohm's law and the Lorentz force law, the induced eddy current density on the conducting sheet is

$$\vec{J} = \sigma\left(\vec{E} + \vec{B} \times \vec{u}\right) = \sigma\left(\vec{E} + \vec{v} \times \vec{B}\right) \tag{1}$$

Fig. 3. The copper guide rail.

Fig. 4. The U-type fixture.

where σ is the conductivity of the conductor and $\vec{v} = -\vec{u}$ is the motion of the conducting plate relative to the moving magnet. The drag force produced by electromagnetic interaction can be calculated as

$$\vec{F}_d = \int_V \vec{J} \times \vec{B} dV \tag{2}$$

From [6], the magnitude of the drag force is $F_d = \alpha\left(\sigma\delta B_0^2 lw\right)v$, where δ is the thickness of the conductor, B_0 is the flux density in the magnetic pole projection area on the conducting sheet, l and w represent the length and width of the pole projection area created by the rectangular permanent magnet and α is defined as [7]

$$\alpha = 1 - \frac{1}{2\pi}\left[4\tan^{-1}\frac{l}{w} + \frac{l}{w}\ln\left(1+\frac{w^2}{l^2}\right) - \frac{w}{l}\ln\left(1+\frac{l^2}{w^2}\right)\right] \tag{3}$$

The drag force $F_d = \alpha\left(\sigma\delta B_0^2 lw\right)v$ with the parameter α defined in Eq. (3) is derived based on the assumption of an infinite conducting plate [6]. For finite dimensional conducting plate, eddy

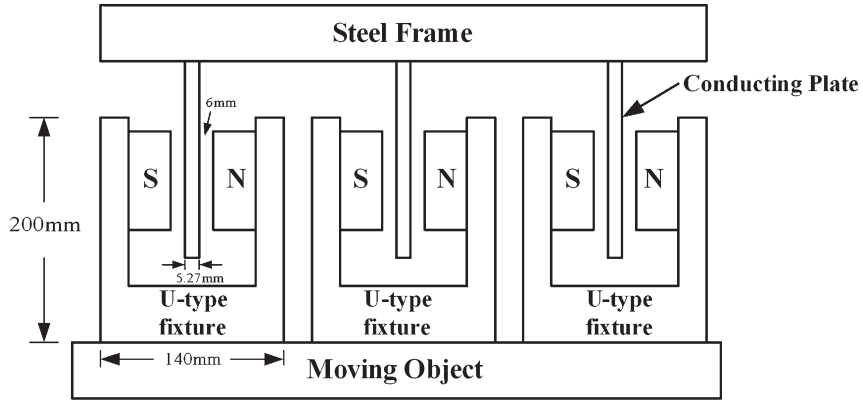

Fig. 5. The cross-section view of the braking medium.

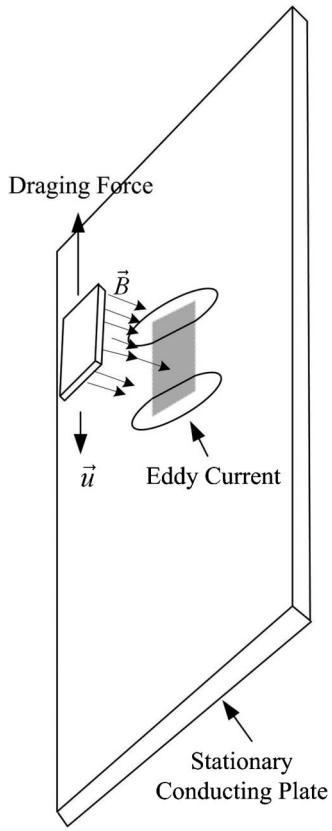

Fig. 6. A permanent magnet moving along a stationary conducting plate.

current in horizontal direction at the boundary of the conducting plate is zero. Therefore, certain modifications to the current density model are necessary. From the results in [7], the drag force is modified to $F_d = \bar{\alpha}\left(\sigma\delta B_0^2 lw\right)v$ with $\bar{\alpha}$ defined as $\bar{\alpha} = \alpha - \alpha_R - \alpha_L$ which is also a constant for a particular design. Details of the parameters are provided in the Appendix. Since $\bar{\alpha}$ is also a constant for a fixed configuration, the drag force $F_d = \alpha\left(\sigma\delta B_0^2 lw\right)v$ will be used for the optimal design in the study to avoid complexity of notations.

Using the mechanism described above, the requirement of the proposed braking system is to decelerate a mass weighing 250 kg dropping from a height of 3 meters. This experiment assumes that the terminal speed (v_f) of the mass is 1 m/sec., and the impact of this speed can be absorbed by some mechanism. Thus, the problem is simplified to finding the strength of the magnetic field which interact with eddy current and induce deceleration equals negative of gravity acceleration at that speed. When the magnetic decelerated force equals the weight of the body impacting the absorber, the mass (m) moves with the final speed (v_f) that is

$$a_B = \frac{F_D}{m} = \frac{5.8\alpha\sigma\delta B^2 wLv_f \times 10^7}{m} \tag{4}$$

where F_D is the magnetic decelerated force, a_B is the deceleration, α is the constant, $\bar{\sigma}$ is the conductivity of the conductor in % IACS[8], δ is the thickness of the conductor, w is the width of the magnet, L is the length of the magnet, and these variables have the following values:

$\alpha = 0.2609$

$\bar{\sigma} = \%\text{IACS}$[8] (The conductivity of copper, $5.8 \times 10^7 \frac{1}{\Omega m}$)

$\delta = 0.006\ m$

$w = 0.143\ m$

$L = 0.435\ m$

$m = 250\ kg$

Therefore, for the terminal speed to equal 1 *m/sec*, where the deceleration equals the gravity acceleration, the strength of the magnetic field is 0.6588 *Tesla* (*T* for short). In [7], the analytical

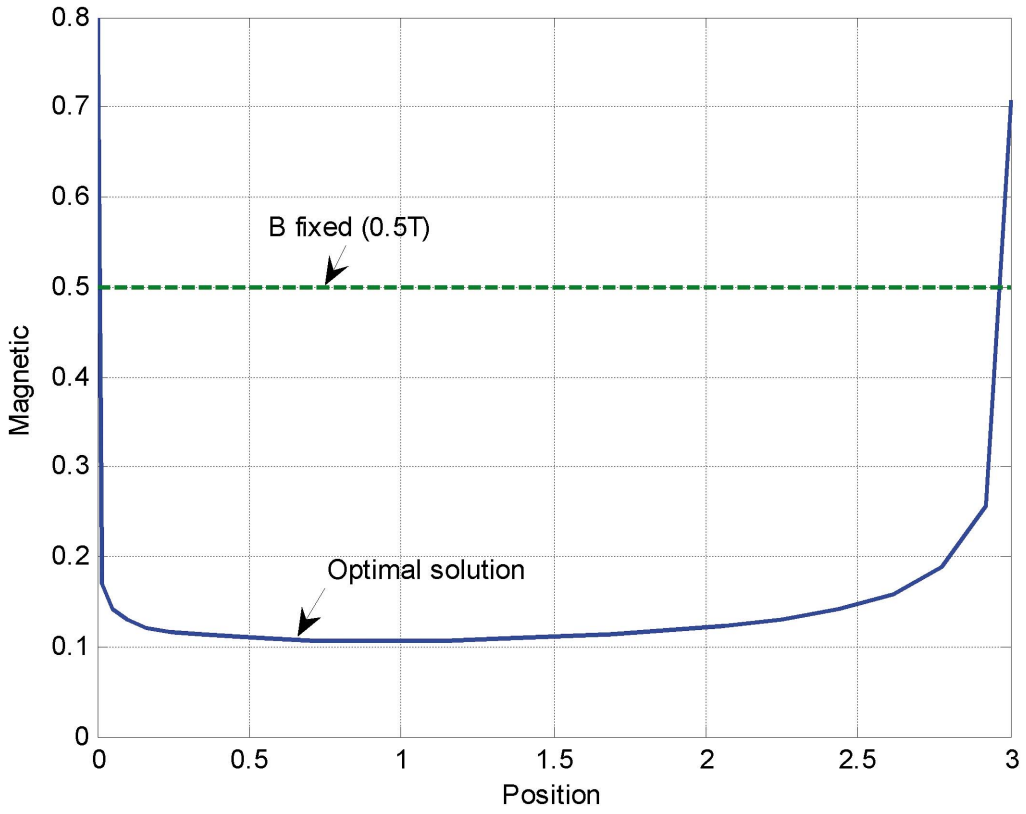

Fig. 7. The optimal magnetic field strength versus position.

model has been verified to reasonably represent the behavior of the eddy current distributions and dynamics of the motion.

3. THE OPTIMIZATION OF THE MAGNETIC FIELD

Since there is no contact between the guide rail and the mass assembly, only gravity and magnetic braking forces are acting on the mass. The magnetic braking force can be expressed in vector form as:

$$\vec{F}_D = -5.8\alpha\bar{\sigma}\delta B^2 wLv \times 10^7 \vec{j} \tag{5}$$

The negative sign indicates that the direction of the force is opposite to the direction of the motion. The factors that influence the magnitude of the force include the material of the permanent magnet (in terms of the density of magnetic flux), the shape of the magnet (in terms of the distribution of the magnetic field), the area of the reaction, the gap between the magnet and the conductor, the shape and the thickness of the conductor, the relative sizes of the magnet and the conductor, the conductivity of the conductor, and the relative velocity of the magnet and the conductor. The equation of the motion in scalar form is given by

$$m\ddot{x} = mg - F_D \tag{6}$$

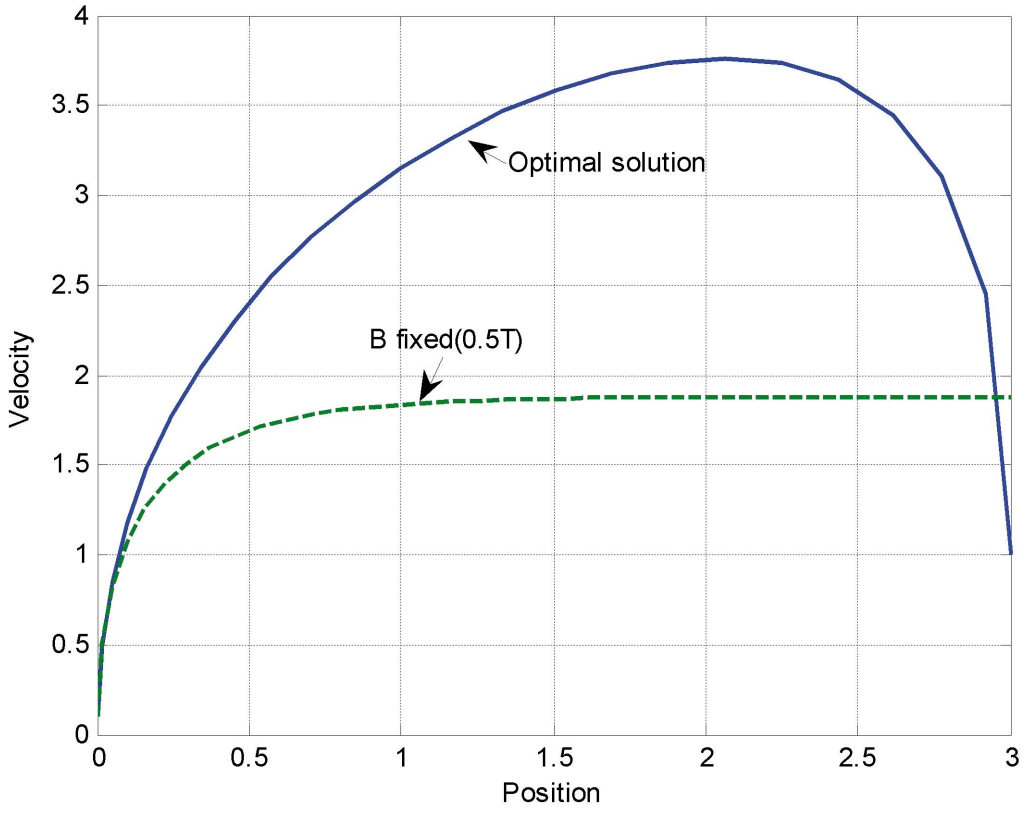

Fig. 8. The velocity versus position for the optimal solution.

or

$$\ddot{x} = g - \frac{F_D}{m} \tag{7}$$

Substituting F_D from Eq. (5) into Eq. (7), leads to

$$\ddot{x} = g - \frac{5.8\alpha\bar{\sigma}\delta B^2 wLv \times 10^7}{m} \tag{8}$$

The state equation form of Eq. (8) is

$$\begin{aligned} \dot{x}_1 &= x_2 \\ \dot{x}_2 &= g - \frac{5.8\alpha\bar{\sigma}\delta B^2 wLx_2 \times 10^7}{m} \end{aligned} \tag{9}$$

To minimize the deceleration effort, the performance index is defined as

$$\min J = \int_0^{t_f} a_B^2 dt \tag{10}$$

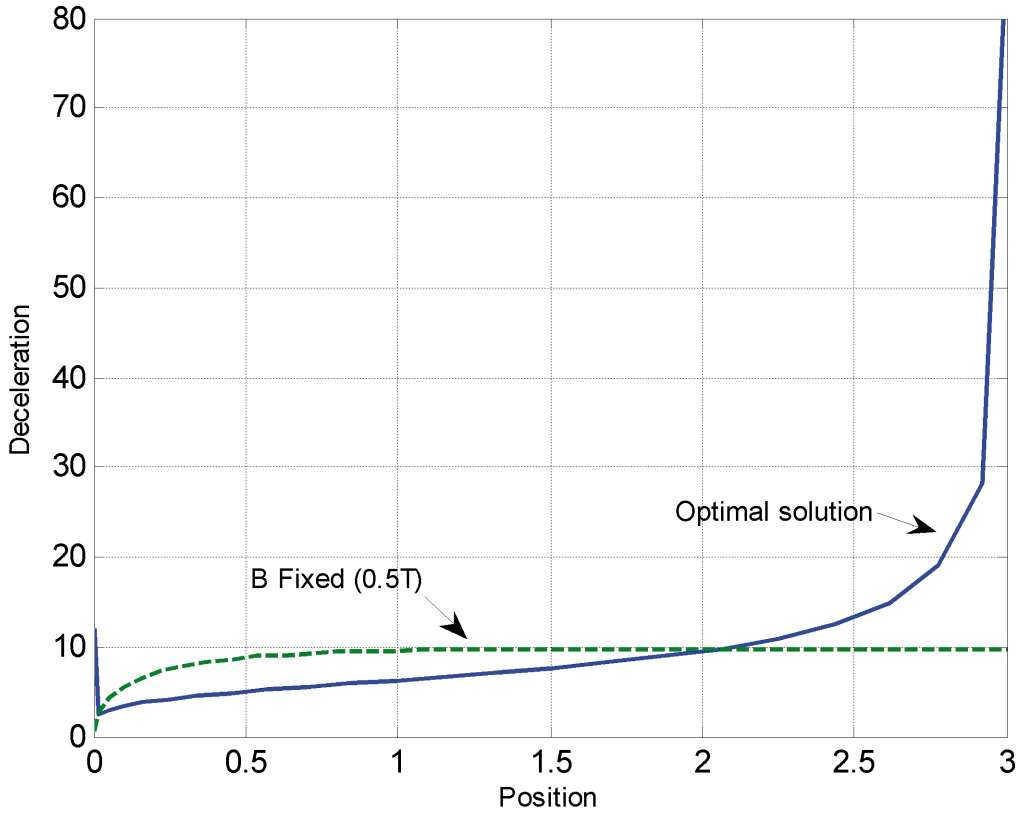

Fig. 9. The deceleration versus position for the optimal solution.

where a_B is the deceleration. By the necessary conditions for optimality [9,10], the Hamiltonian is then given by

$$H = p_1 x_2 + p_2 \left(g - \frac{5.8\alpha\bar{\sigma}\delta B^2 w x_2 \times 10^7}{m} \right) + (a_B)^2 \tag{11}$$

With the deceleration a_B given by the Eq. (4), the Hamiltonian can further be written as

$$H = p_1 x_2 + p_2 \left(g - \frac{5.8\alpha\bar{\sigma}\delta B^2 w x_2 \times 10^7}{m} \right) + \left(\frac{5.8\alpha\bar{\sigma}\delta B^2 w L x_2 \times 10^7}{m} \right)^2 \tag{12}$$

and the co-state equations become

$$\begin{aligned} \dot{p}_1^* &= -\frac{\partial H}{\partial x_1} = 0 \\ \dot{p}_2^* &= -\frac{\partial H}{\partial x_2} = -p_1 + p_2 \left(\frac{5.8\alpha\bar{\sigma}\delta B^2 w L \times 10^7}{m} \right) - 2 \left(\frac{5.8\alpha\bar{\sigma}\delta B^2 w L \times 10^7}{m} \right)^2 x_2 \end{aligned} \tag{13}$$

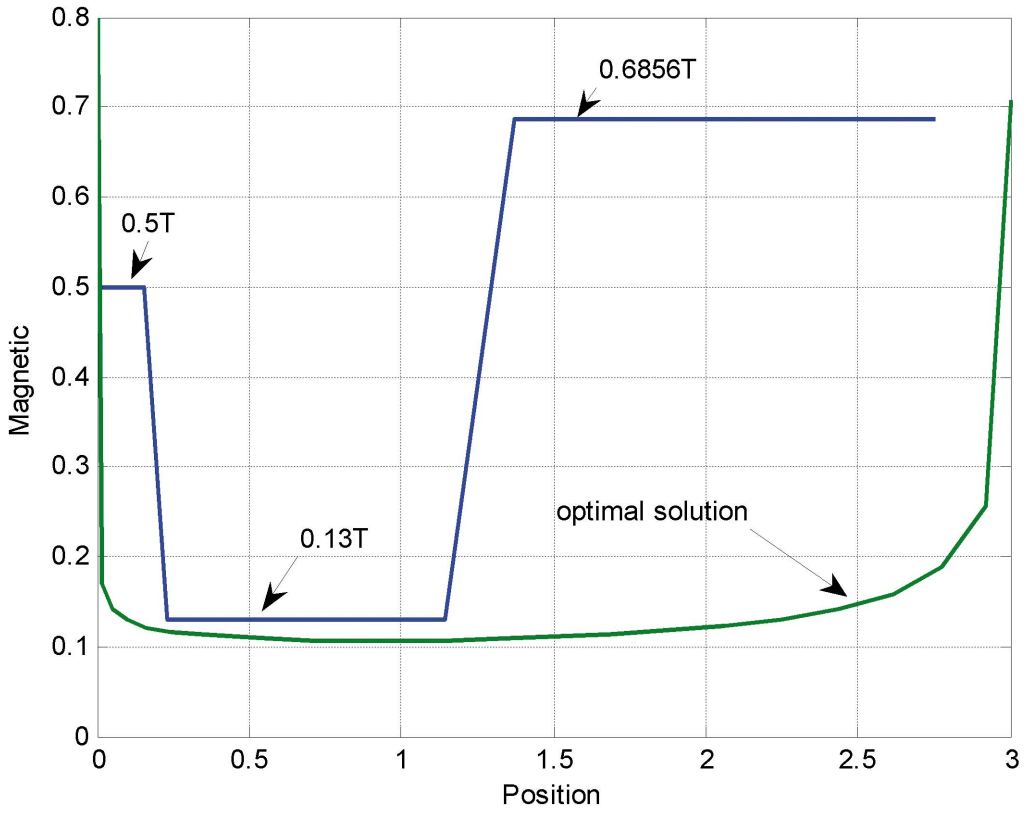

Fig. 10. The piecewise-constant magnetic field strength versus position.

If the magnitude of the magnetic field B is the control and is assumed to be unbounded, the optimal control can be obtained from the equation:

$$\frac{\partial H}{\partial B}=0 \tag{14}$$

Performing the differentiation, yields

$$\frac{\partial H}{\partial B}=-2p_2\left(\frac{5.8\alpha\bar{\sigma}\delta wL\times 10^7}{m}x_2\right)B+4\left(\frac{5.8\alpha\bar{\sigma}\delta wL\times 10^7}{m}x_2\right)^2B^3=0 \tag{15}$$

Solving for the optimal control of the magnetic field leads to

$$B=\pm\sqrt{\frac{0.5p_2m}{5.8\alpha\bar{\sigma}\delta wLx_2\times 10^7}} \tag{16}$$

Since the negative magnetic field strength is irrelevant, the positive sign is reserved. Substituting the optimal magnetic field control into Eqs. (9) and (13), we have

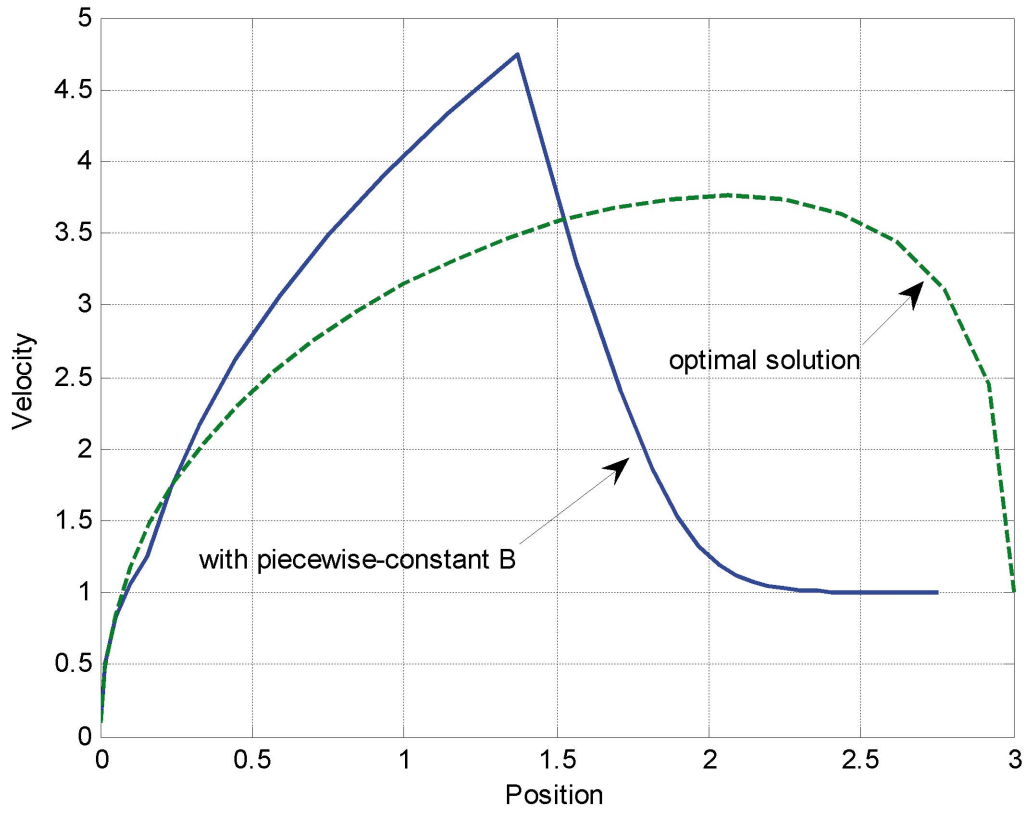

Fig. 11. The velocity versus position for the piecewise-constant magnetic field strength.

$$\begin{aligned}
\dot{x}_1 &= x_2 \\
\dot{x}_2 &= g - \frac{p_2}{2} \\
\dot{p}_1 &= 0 \\
\dot{p}_2 &= -p_1 + \frac{p_2^2}{2x_2}
\end{aligned} \tag{17}$$

Referring to the physical situation, we have the following boundary conditions:

When $t = 0$,

$$\begin{aligned}
x_1(0) &= 0, \\
x_2(0) &= 0.
\end{aligned} \tag{18}$$

When $t = t_f$,

$$\begin{aligned}
x_1(t_f) &= 3 \\
x_2(t_f) &= v_f = 1\ m/\text{sec}.
\end{aligned} \tag{19}$$

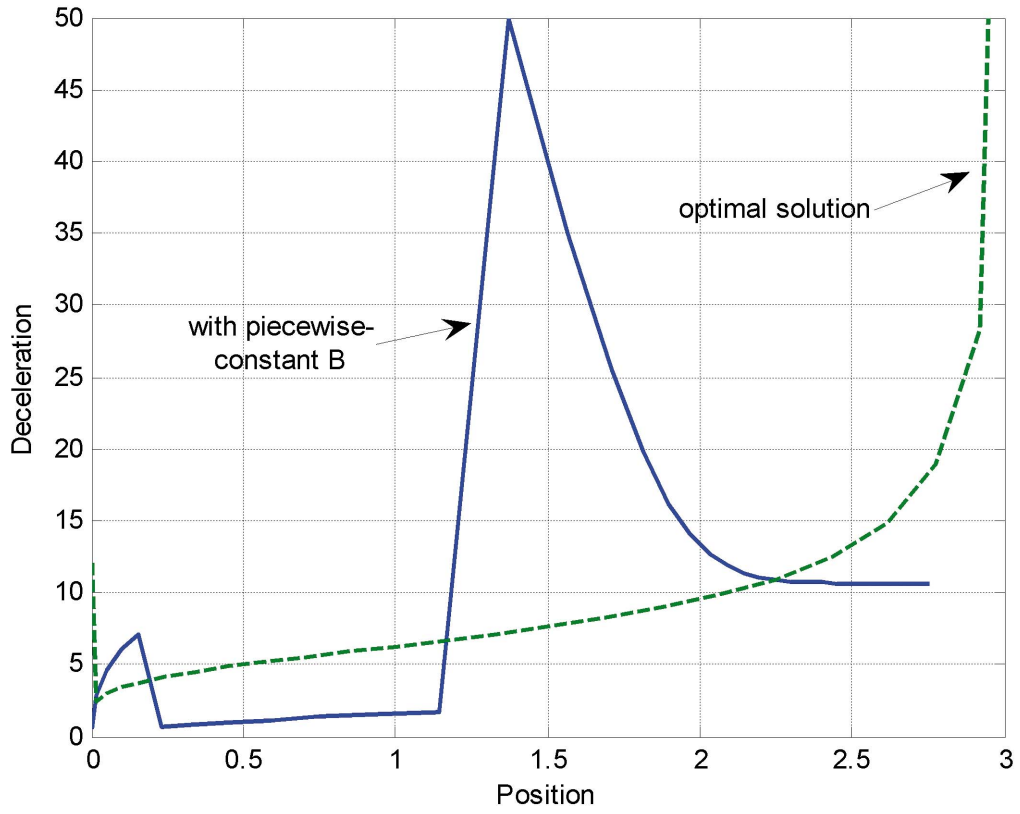

Fig. 12. The deceleration versus position for the piecewise-constant magnetic field strength.

Since $B=\sqrt{\dfrac{0.5p_2m}{5.8\alpha\bar{\sigma}\delta wLx_2\times 10^7}}$, the magnetic field is infinite when $x_2 = 0$ (initial speed equals to zero). To avoid this situation, we provided the mass with an initial speed of 0.1 *m/sec.* as it entered the reaction zone. Therefore, the boundary condition (18) is

$$\begin{aligned} x_1(0)&=0\\ x_2(0)&=0.1 \end{aligned} \tag{20}$$

The final time t_f is un-specified, and all the final states are given. By the transversality condition [9,10] , and since time is not explicitly contained in the Hamiltonian, hence

$$H=0 \tag{21}$$

We need four initial conditions to solve Eq. (17). Equation (20) gives two of these conditions, x_{10} and $x_{20,}$ but, p_{10} and $p_{20,}$ are still needed. Using the shooting method [11], which is a method for solving a boundary value problem by reducing it to the solution of an initial value problem, we guess the values of p_{10} and p_{20} and integrate Eq. (17). Comparing the final values of x_1 and x_2 with the boundary condition Eq. (19), if they are equal in some interval, then we have the optimal solution. If they are not, it is necessary to guess the initial values of p_{10} and p_{20} and repeat the procedure.

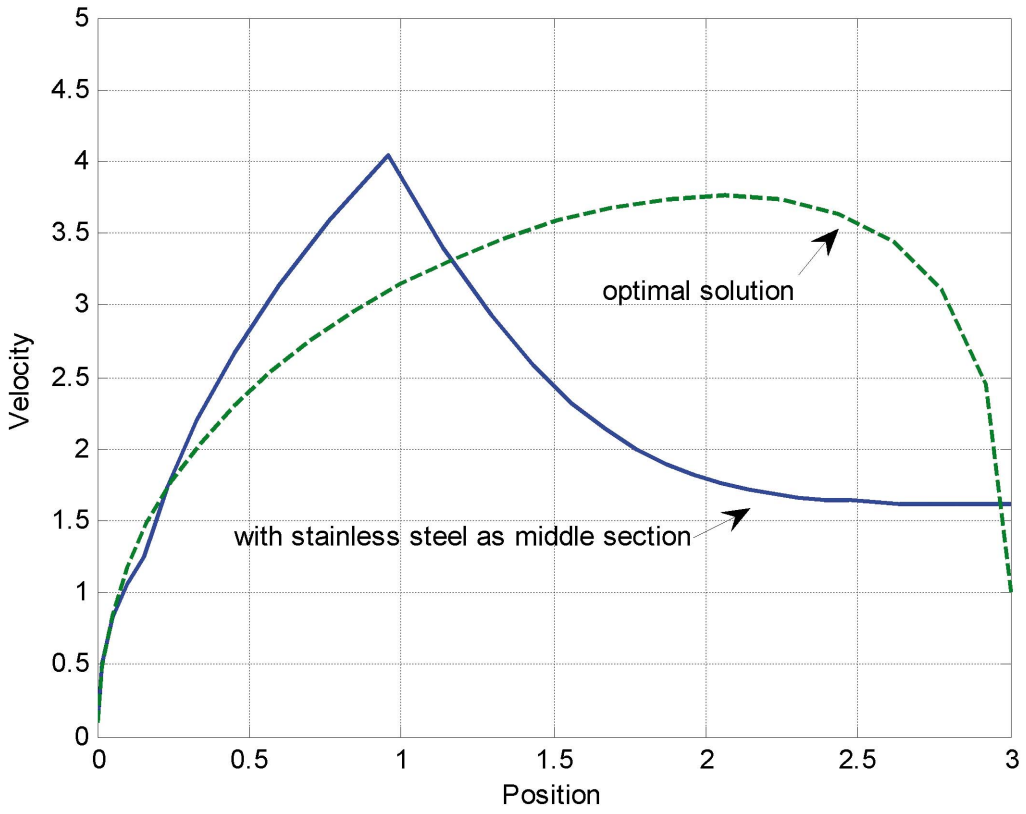

Fig. 13. The velocity versus position with the stainless steel as middle section.

Figures 7–9 are the plots of the magnetic field strength, velocity, and deceleration versus position for the optimal solution. Simulation results show that the velocity requirement at the end of rail is achieved. The strength of the magnetic field is about 0.12 T which is lower than that of constant magnetic field. As expected, the strength rises quickly when the mass reaches the bottom. To meet magnetic field requirement, the proposed design uses an electrical magnet. Therefore, the current varies according to the position of the mass. Near the end, the current rises quickly. Besides, the deceleration reaches approximately 9 g.

4. THE PIECEWISE-CONSTANT MAGNETIC FIELDS AND SECTION-WISE GUIDE RAIL

To avoid the disadvantages of high current required and deceleration generated, and refer to the optimal magnetic field distribution, this study also proposes a piecewise-constant magnetic field strength approach. To approximate the optimal magnetic strength distribution, a section with the magnetic strength of 0.5 T with arbitrary length is chosen, followed by $B = 0.13$ T. Since the condition of constant terminal speed determines the magnetic strength of last section to equal 0.6856 T. The lengths of $B = 0.13$ T and $B = 0.6856$ T are adjusted to meet the condition of 1.0 m/sec terminal speed. Figures 10–12 present the simulation results. The results show that the deceleration reaches to approximate 5 g at the middle of the track.

According to Eq. (2), instead of varying the magnetic field according, it is much easier to keep the magnetic field constant and selecting the proper conduct materials. For example, we can

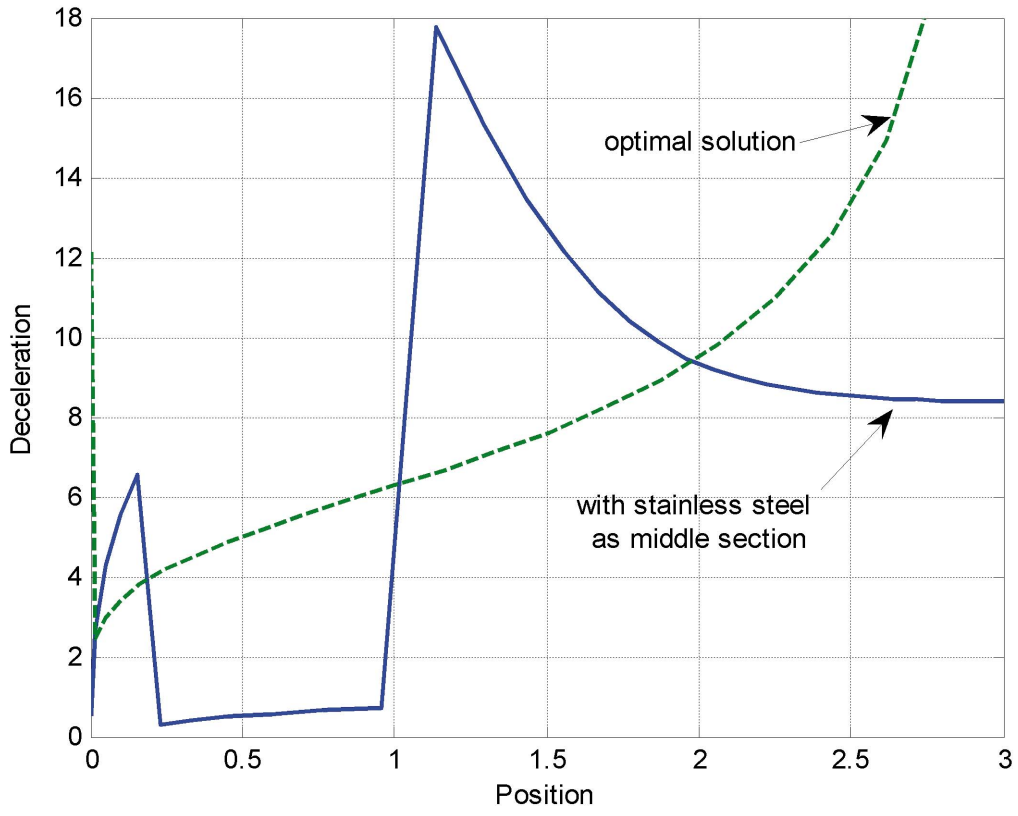

Fig. 14. The deceleration versus position with the stainless steel as middle section.

divide the conductor into three sections. With a constant magnetic field strength of 0.64 T and a terminal speed requirement of 1.0 m/sec, the conductivity required for the last section can be calculated as:

$$\sigma = \frac{mg}{5.8\bar{\alpha}\delta B^2 wLv \times 10^7} = \frac{250(9.8)}{0.2609(0.006)(0.64)^2(0.143)(0.435)(1.0)} \Big/ \left(5.8 \times 10^7\right) = 105.9\ \%\text{IACS} \tag{22}$$

Referring to the physical properties of the materials [8], silver has the conductivity of 105.7 %IACS and offers the closest matching conductivity. To simplify the design, we chose copper as the conductor in the first section. The design parameters left to determine are the material of the second section and the relative lengths of the conductors. These can be determined by letting the maximum deceleration not exceed 2 g. Two alternatives are proposed. For the first configuration, copper, stainless steel (Chromium Nickel), and silver are selected for the first, second, and third sections, respectively. For the second configuration, stainless steel is replaced by carbon steel (plain carbon 0.45 %) in second section. From [8], the conductivities for stainless steel and carbon steel are 3 % IACS and 10 % IACS respectively. Figures 13–16 present these simulation results. In both cases, the maximum deceleration is reduced to approximately 2 g which is tolerable for the general public [12]. Since the conductivity of silver which is used for the last section is not exact equal the required conductivity given by Eq. (22), the terminal

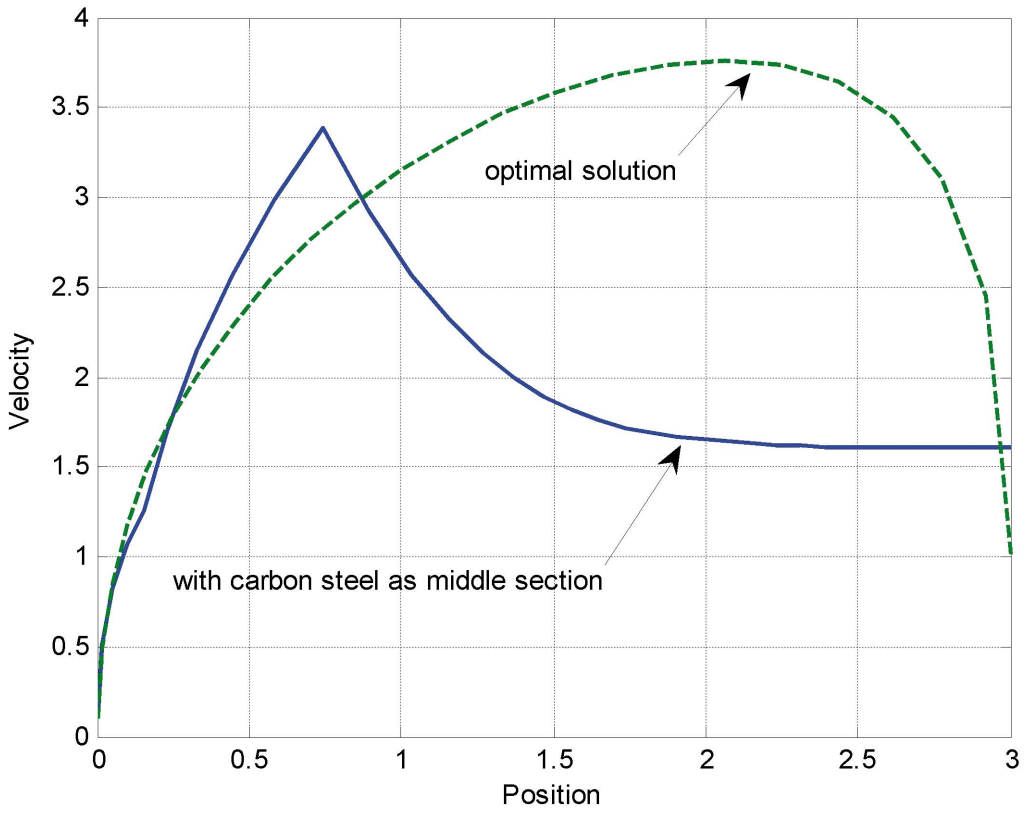

Fig. 15. The velocity versus position with the carbon steel as middle section.

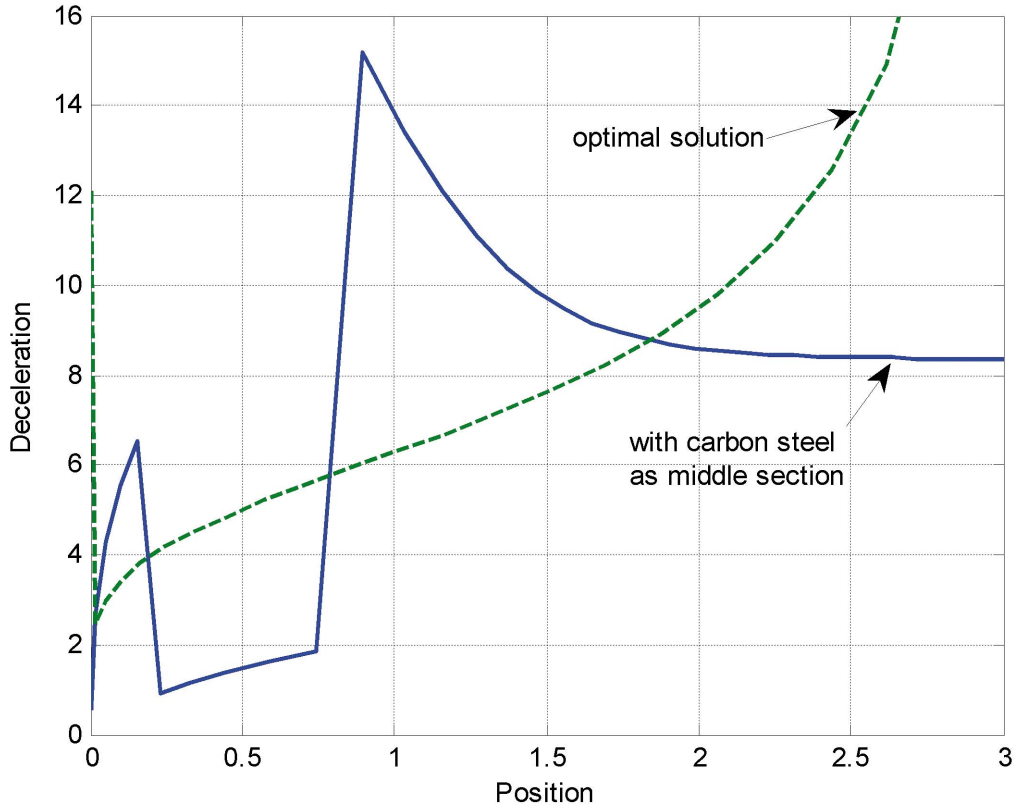

Fig. 16. The deceleration versus position with the carbon steel as middle section.

speed is not equal to 1.0 *m*/*sec*. For clearer demonstration, the velocity profiles for different configurations are shown in Fig. 17.

5. CONCLUSIONS

The design of eddy current brakes is presented in the paper. Eddy current brakes provide non-contact means to produce braking forces required to decelerate the motion of a moving object. In this study, four systematic engineering design scenarios to design a braking system are presented: a constant magnetic field, an optimal magnetic field distribution, piecewise-constant magnetic fields and a section-wise guide rail with a constant magnetic field. Although the simulation results above show that the optimal magnetic field is better than the constant magnetic field, a deceleration peak of 9 *g* it is not suitable for most people. Further, the sudden increase in current could cause wire overload. The piecewise constant magnetic field has the advantages of a preset terminal speed and predictable wire current but it produces a higher speed. Alternatively, it is much easier to keep the magnetic field constant and select the proper conductor materials. The advantages of these last two designs using different materials along the guide rail are tolerable deceleration; and easy manufacturing. A nearly maintenance-free system can be achieved if permanent magnet is utilized to establish the magnetic field.

It should be noted that the simulation results show in the paper are based on the assumption of using infinite conducting plate. For finite dimensional conducting plate, the required magnetic field has to be increased so that the same design results (velocity and deceleration) can be maintained. The amount of increase on the magnetic field depends on the physical dimension

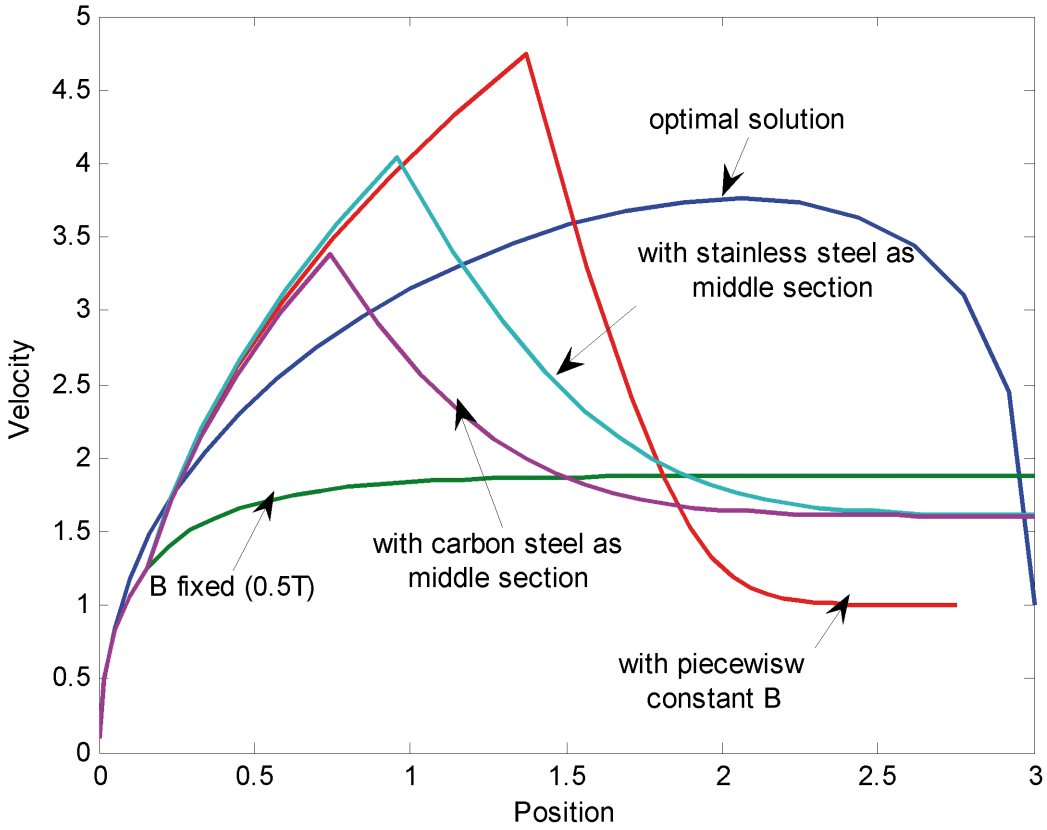

Fig. 17. Comparison of the velocity profiles for different design configurations.

of the conducting plate. For the experimental system presented in the paper, a 31 % increase is required when the image method is used to compute the drag force.

ACKNOWLEDGEMENT

Part of the study was sponsored by the First Division, Chung-Shan Institute of Science and Technology, Taiwan, Republic of China, under the contract number XW90138-P101P00.

REFERENCES

1. Gagarin, G., Kroger, U. and Saunweber, E., "Eddy-current magnetic track brakes for high-speed trains," *Joint ASME/IEEE/AAR Railroad Conference*, pp. 95–99, 1987.
2. Ohyma, T., "Adhesion at higher speeds, its basic characteristic, its improvement and some related problem," *Japanese Railway Engineering*, Vol. 108, 1988.
3. Mcconnell, H.M., "Eddy-current phenomena in ferromagnetic material," *AIEE Transactions*, Vol. 73, part I, pp. 226–234, July, 1954.
4. Kesavamurthy, N., "Eddy-current in solid iron due to alternating magnetic flux," *The Institution of Engineers Monograph*, No. 339U, pp. 207–213, June, 1959,
5. Biro, O. and Preis, K., "Finite element analysis of 3-D eddy current," *IEEE Transactions on Magnetics*, Vol. 26, No. 2, pp. 418–423, Mar, 1990.
6. Heald, M.A., "Magnetic braking: improved theory," *American Journal of Physics*, Vol. 56, No. 6, pp. 521–522, 1988.

7. Jaw-Kuen Shiau, Der-Ming Ma, and Min Jou, "Analysis and experiments of eddy current brakes with moving magnets," *Materials Science Forum*, Vols. 575–578, pp. 1299–1304, 2008.
8. Ross Robert, B, *Metallic Materials Specification Handbook*, 4th edition, Springer, 1991.
9. Donald E. Kirk, *Optimal Control Theory: An Introduction*, Prentice-Hall, 1970.
10. Frank L. Lewis and Vassilis L. Syrmos, *Optimal Control*, 2nd edition, John Wiely & Sons, 1995.
11. Josef Stoer and Roland Bulirsch, *Introduction to Numerical Analysis*, Springer-Verlag, 1980.
12. James F. Parker and Vita R. West, *Bioastronautics Data Book*, 2nd edition, NASA SP-3006, 1973.

APPENDIX

Consider the structure depicted in Fig. A1, the boundaries of the conducting plate are at $x=A$ on the right and $x=-B$ on the left. The length of the plate is considered much longer than the length of the magnet. Because eddy current in x-direction is zero at the left and right boundaries of the conducting plate, the image method assumes that imaginary eddy currents exist on the left and right hand sides of the finite dimensional conducting plate that render the net eddy currents at left and right boundaries of the conducting plate to zero. Figure A2 represents the eddy current distribution at $y=0$. The symmetric axes $x=R_s$ for right imaginary eddy current and $x=-L_s$ for left imaginary eddy current are determined according to the boundary conditions, i.e., eddy current in x-direction is zero at the left and right boundaries of the conducting plate. Under these assumptions, the drag force can be expressed as $F_d=\bar{\alpha}\left(\sigma\delta B_0^2 lw\right)v$, where $\bar{\alpha}=\alpha-\alpha_R-\alpha_L$. The parameters α_R and α_L are defined as

$$\alpha_R=-\frac{1}{\pi lw}(M_R+N_R),\ \alpha_R=-\frac{1}{\pi lw}(M_L+N_L)$$

with

$$M_R=l(R_s-w)\tan^{-1}\frac{l}{R_s-w}-R_s l\tan^{-1}\frac{l}{R_s}-\frac{1}{4}R_s^2\ln R_s^2+\frac{1}{4}(R_s-w)^2\ln(R_s-w)^2$$
$$+\frac{1}{4}\left(R_s^2-l^2\right)\ln\left(R_s^2+l^2\right)+\frac{1}{4}\left[l^2-(R_s-w)^2\right]\ln\left[l^2+(R_s-w)^2\right]$$

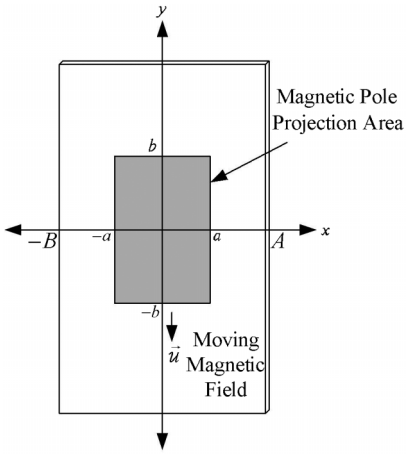

Fig. A1. Configuration of a moving magnetic field on a stationary conducting plate.

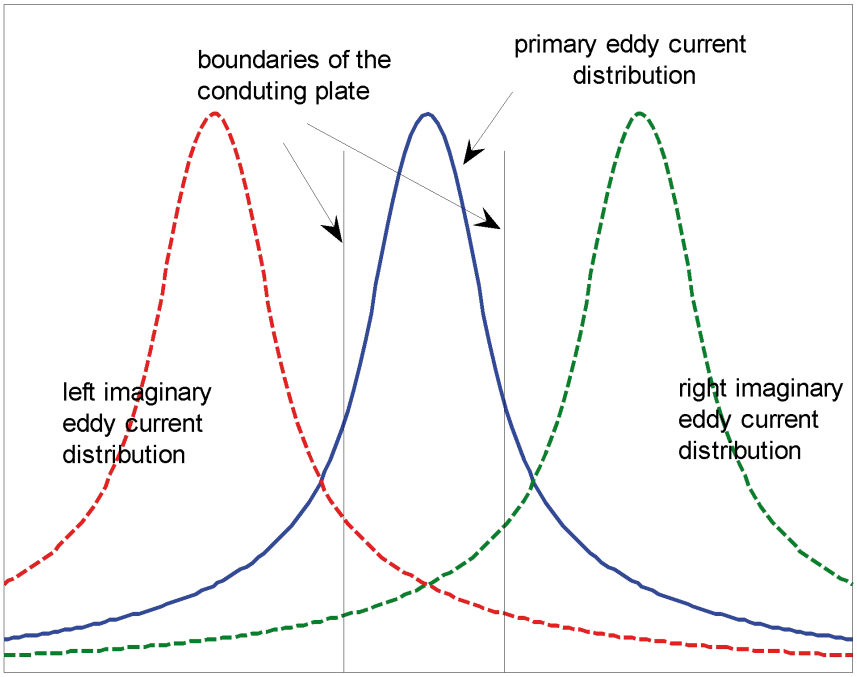

Fig. A2. Eddy current distribution for a finite width conducting plate.

$$N_R = l(R_s+w)\tan^{-1}\frac{l}{R_s+w} - R_s l\tan^{-1}\frac{l}{R_s} - \frac{1}{4}R_s^2\ln R_s^2 + \frac{1}{4}(R_s+w)^2\ln(R_s+w)^2 + \frac{1}{4}\left(R_s^2-l^2\right)\ln\left(R_s^2+l^2\right) + \frac{1}{4}\left[l^2-(R_s+w)^2\right]\ln\left[l^2+(R_s+w)^2\right]$$

$$M_L = l(L_s+w)\tan^{-1}\frac{l}{L+w} - L_s l\tan^{-1}\frac{l}{L_s} - \frac{1}{4}L_s^2\ln L_s^2 + \frac{1}{4}(L_s+w)^2\ln(L_s+w)^2 + \frac{1}{4}\left(L_s^2-l^2\right)\ln\left(L_s^2+l^2\right) + \frac{1}{4}\left[l^2-(L_s+w)^2\right]\ln\left[l^2+(L_s+w)^2\right]$$

$$N_L = l(L_s-w)\tan^{-1}\frac{l}{L_s+w} - L_s l\tan^{-1}\frac{l}{L_s} - \frac{1}{4}L_s^2\ln L_s^2 + \frac{1}{4}(L_s-w)^2\ln(L_s-w)^2 + \frac{1}{4}\left(L_s^2-l^2\right)\ln\left(L_s^2+l^2\right) + \frac{1}{4}\left[l^2-(L_s-w)^2\right]\ln\left[l^2+(L_s-w)^2\right]$$